ECS Advances

The Electrochemical Society
Advancing solid state & electrochemical science & technology

OPEN ACCESS

Electrochemical Performance of a Spatially Distributed ECPrOx Reactor

To cite this article: Ivonne Karina Peña Arias *et al* 2023 *ECS Adv.* **2** 034501

View the article online for updates and enhancements.

You may also like

- Electrochemical Preferential Oxidation of CO in Reformate
Jingxin Zhang and Ravindra Datta
- Nitrogen-Doped Graphene Supported - $Co(OH)_2$ for Sensitive Determination of Adrenaline
Abdul Kader Mohiuddin and Seungwon Jeon
- The Identification of Degradation Parameters in SOC Under Load and OCV Aging Approaches
Aiswarya Padinjarethil and Anke Hagen

We Advance Battery Research!

EL-CELL®
electrochemical test equipment

- Electrochemical Battery Test Cells
- Multi-channel Potentiostats / Galvanostats / EIS
- Tools, Consumables & Testing Services

el-cell.com +49 40 79012-734 sales@el-cell.com

This content was downloaded from IP address 2.201.94.40 on 05/10/2023 at 15:37

ECS Advances, 2023 **2** 034501

Electrochemical Performance of a Spatially Distributed ECPrOx Reactor

Ivonne Karina Peña Arias,[1] Richard Hanke-Rauschenbach,[2,z] and Kai Sundmacher[1,3]

[1]*Process Systems Engineering, Otto-von-Guericke University Magdeburg, Universitätsplatz 2, 39106 Magdeburg, Germany*
[2]*Electric Energy Storage Systems, University of Hannover, Appelstr. 9A, 30167 Hannover, Germany*
[3]*Max Planck Institute for Dynamics of Complex Technical Systems, Sandtorstr. 1, 39106 Magdeburg, Germany*

In this contribution a spatially distributed Electrochemical Preferential Oxidation (ECPrOx) reactor is evaluated and the influence of the temperature, CO inlet concentration, feed flow rate and relative humidity on the polarization curve, the local current distribution and the CO outlet concentration, selectivity and conversion are investigated. For that, six different cases are studied under galvanostatic and potentiostatic operation. For Galvanostatic operation, it was observed that depending on the operation conditions, the bifurcation point as well as the frequency and amplitude of the oscillations can be modified. Additionally, several spatiotemporal profiles of the local current density were found. For potentiostatic operation, the spatiotemporal profiles are constant with time, however they are affected by the anode overvoltage. Finally, after the bifurcation point, the temporal averaged anode overvoltage and the CO outlet concentration is always lower for galvanostatic control.

© 2023 The Author(s). Published on behalf of The Electrochemical Society by IOP Publishing Limited. This is an open access article distributed under the terms of the Creative Commons Attribution 4.0 License (CC BY, http://creativecommons.org/licenses/by/4.0/), which permits unrestricted reuse of the work in any medium, provided the original work is properly cited. [DOI: 10.1149/2754-2734/acec00]

Manuscript submitted January 12, 2023; revised manuscript received June 27, 2023. Published August 9, 2023.

The electrochemical preferential oxidation (ECPrOx) reactor has been proposed and investigated as a technical application of the autonomous potential oscillations that arise due to the presence of carbon monoxide (CO) in polymer electrolyte membrane fuel cells (PEMFC).[1–5] The oscillations are a self-cleaning mechanism of the cell, which are found when operated under current control.[6–15] Under potentiostatic operation, oscillations have not been reported, however a significantly high performance drop is observed when compared to a standard PEMFC.[16]

A review of the literature available for CO poisoning and the mitigation strategies for PEMFCs was recently published by Ref. 17. They give a wide overview in the mechanisms and the influence of the operating parameters on the fuel cell behavior. The main parameters investigated are temperature, current density, type of catalyst, flow rate and relative humidity.[6,10,11,13,18] A more general review on the poisoning effects, mechanism and mitigation strategies for PEMFC was also recently prepared by Ref. 19 including a section focusing on the impact of CO and carbon dioxide.

Analogously to the Preferential Oxidation reactor (PrOx), where hydrogen produced in a reforming step is used as feedstock; in an ECPrOx reactor the purpose is to selectively oxidize the carbon monoxide traces so that the hydrogen is purified and can be further used in a PEMFC. A technical evaluation of such a system has been carried out by different researchers[1–4,20,21] and a summary of their main findings can be found in Ref. 5; where they also published a systematic study of the influence of the oscillations on the CO conversion and the selectivity in a well-mixed ECPrOx reactor.

Furthermore, in the modeling and experimental studies from Ref. 2–4, 22 it has been observed that the selectivity and conversion of the reactor increases when a sequence of well mix reactors are connected in series without electrical coupling. When the electrical coupling is present, the selectivity and conversion slightly decrease but they are still higher than for a single well mixed reactor. Such a reactor can be technically realized when the geometry of the cell is designed in such a way that it can emulate a Plug Flow Tubular Reactor (PFTR). According to the simulations and modeling results of Ref., [9,12] spatiotemporal patterns are formed for a range of wide technical relevant operating conditions.

In 2013, Kirsch et al.[11] published an experimental study where the formation of complex spatiotemporal patterns was confirmed for galvanostatic and potentiostatic operation. For this, they carried out current and voltage scans on a spatially distributed cell, which was fed with hydrogen and CO traces. As operating parameters, they varied the anode feed flow rate and the CO inlet concentration. They found that under galvanostatic operation, when the cell is well humidified and the feed flow rate is high, the local current and overpotential oscillates at a single frequency. On the contrary, when the feed flow rate is reduced, a second main frequency arises. This phenomenon was named *period doubling* bifurcation. Furthermore, under potentiostatic control, the presence of pulses in the spatiotemporal patterns was observed.

So far, a systematic evaluation of a spatially distributed ECPrOx reactor has not been carried out. Also unknown is the relation between the spatiotemporal patterns and the CO outlet concentration, selectivity and conversion. Therefore in this study, the behavior of an ECPrOx reactor with a straight channel design is experimentally evaluated. The temperature, feed flow rate, CO inlet concentration and relative humidity were varied and a complete polarization curve under galvanostatic and potentiostatic operation was evaluated for all scenarios. For each experiment, the local current density and the CO outlet concentration were measured, so that the formation of spatiotemporal patterns and their impact in the CO outlet concentration can be determined. Furthermore, the conversion, selectivity and the specific energy required for the CO oxidation were evaluated for all scenarios.

This contribution is organized as follows: in the following section, the spatially distributed cell, the equipment, the materials, and experimental workflow are described. In Results and Discussion section, the results are shown and discussed. Finally, the conclusions and outlook are presented in Conclusions and outlook sections.

Experimental Setup

In order to determine the spatiotemporal behavior of the reactor, it is required to measure independently the local current at each position; for this, a segmented fuel cell developed by S^{++} Simulation Services was used. Each segment ($l = 1.8$ mm) consists of a shunt of known resistance, which was then integrated into a printed circuit board. The voltage across the shunt resistors is measured and the local current is calculated by applying Ohms law. The total length of the channel is 1440 mm and the flow field consists of six channels; only in the two middle channels the current distribution is measured. The other four channels are foreseen for homogenization purposes, see Fig. 1; more information on the device can be found in Ref. 13. The minimum sampling time between measurements of the local current density profiles was 10 ms and the active cell area was 32 cm^2.

[z]E-mail: hanke-rauschenbach@ifes.uni-hannover.de

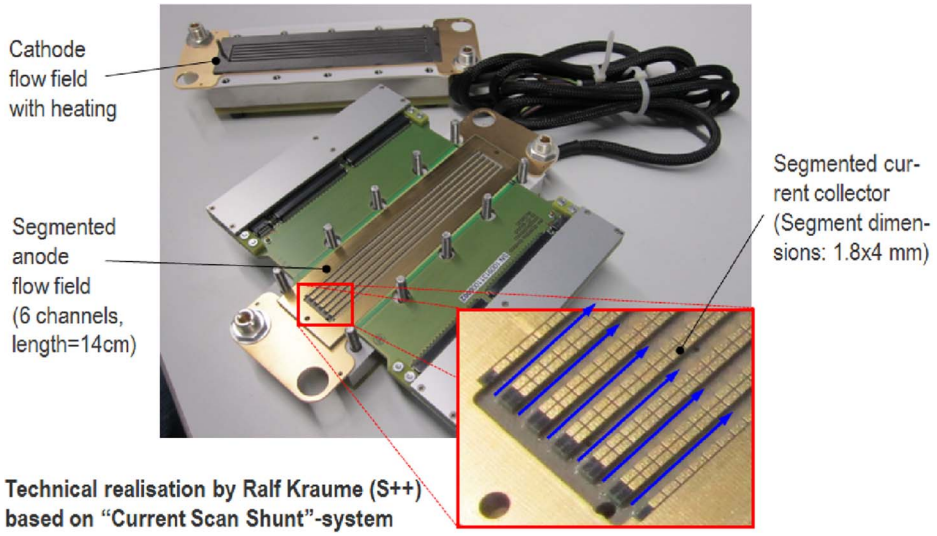

Figure 1. Segmented fuel cell developed by S^{++} Simulation Services. Figure taken from Ref. 13.

The membrane electrode assembly (MEA) was produced in-house; for this, two different catalyst inks were prepared. The weight concentration of the metal catalyst was 70% and 30% was pulverized Nafion. The metal catalyst used for the ink preparation was pure Platinum for the cathode and a mix of Platinum and Ruthenium in equal proportions for the anode. The platinum concentration for both electrodes was 1 mg/cm^2. A detailed description of the ink preparation and the materials is given elsewhere.[5,13] SGL 25 BC gas diffusion layers provided by Solvicore GmbH & Co. KG were attached at the anode and cathode.

A test station produced by FuelCon was used to carry out the experiments. The station is composed of several mass flow controllers and valves for the anode and cathode side where the desired feed flow rate can be easily adjusted and monitored. Afterward, the gases are fed to the bubblers where the gases are saturated with water vapor at the desired temperature. Subsequently, heating hoses allow holding or increasing the temperature of the humidified gases before they enter the cell. After the cell, the exhaust gases are collected and control valves allow modifying and holding the pressure within the cell. Additionally, the station allows to monitor the cell temperature and possess a Hörcherl and Hackl ZS Electronic load that allows operating galvanostatically and potentiostatically. However, since the load is passive and can only consume energy, it is necessary to incorporate an additional energy source, in this case a Statron Power Supply 2257-8.

The gases fed to the cell where purchased from Westfalen AG. For the anode, a Test gas containing 1% carbon monoxide (N2.0) dissolved in hydrogen (N5.0) was diluted with pure hydrogen (N5.0) to obtain the desired inlet concentration of CO. At the cathode, to have a well-defined counter electrode and avoid hydrogen crossover, a mixture of 10% Hydrogen (N5.0) in Nitrogen (N5.0) was selected. The main advantage of such a counter electrode is that the measured potential losses can be attributed to the working electrode.

Once assembled, the cell was electrically shorted and stored before it was used. When connected for the first time, a conditioning procedure was followed to free the catalyst area of contaminants. A description of the procedure was given elsewhere.[23] For every series of experiments, first the polarization curve of the system at the given temperature, relative humidity and feed flow rate was measured with pure hydrogen. With this information, the voltage losses related purely with the CO presence in the anode can be determined as,

$$\eta_A(i) = U_{cell}^{H_2,CO}(i) - U_{cell}^{H_2}(i) \quad [1]$$

with

η_A	Anode overvoltage	[V]
$U_{cell,i}^{H_2,CO}$	Cell voltage with CO traces at a given current	[V]
$U_{cell,i}^{H_2}$	Cell voltage without CO traces at a given current	[V]

After this, the required feed flow rate of the test gas is adjusted, so that the desired CO inlet is achieved. To ensure this, a homogenization period of 40 minutes at open circuit voltage is given to the system so that the catalyst surface is saturated with CO and the inlet concentration equals the outlet. Following that, the exhaust gas of the anode was collected in gas sampling bags (1 L) from Restek GmbH. Subsequently, the CO inlet concentration was measured in an Agilent 6890 chromatograph.

It is known from the works of Lopes and Lu,[20,21] that for galvanostatic operation, the CO outlet concentration oscillates at the same frequency that the voltage does. Since for our experimental scenarios frequencies higher than 0.5 Hz were expected, the CO outlet could not be measured online and instead the temporal averaged CO outlet concentration was determined.

Then the polarization curve for potentiostatic and galvanostatic operation was simultaneously measured. First, the cell voltage was fixed and once the steady-state current was reached (waiting time 20 min) the exhaust gas was collected. Next, the current was set to the already known steady-state current, the same waiting period was given and a new gas sample was collected. These steps were followed until the complete polarization curve was recorded. During the evaluation, the sampling rate for potentiostatic operation was 200 ms and for galvanostatic operation 20 ms.

To determine the anode overvoltage, Eq. 1 can be used for potentiostatic operation and for galvanostatic operation, as long as oscillations are not present. Once the oscillations emerged, the temporal averaged voltage should be first calculated.

To evaluate the technical performance of the reactor, the conversion and selectivity of CO, as well as, the hydrogen recovery ratio and the specific energy required are calculated. For this, the same Eqs. and approached used by Ref., 5 where the authors have given an extended explanation for the formulas derivations, are here applied. In this work, only a brief presentation of the formulas is given.

Knowing the inlet and averaged outlet CO concentration, the CO conversion can be calculated as the ratio between the total amount of CO averaged converted and the total amount of CO at the inlet of the

reactor. However, since the chromatographic evaluation is carried out at room temperature, the molar flow should be corrected to account for water condensation,

$$X_{CO} = \frac{g^*_{in,A} x^{CO}_{in} - g^*_{out,A} x^{CO}_{out}}{g^*_{in,A} x^{CO}_{in}} \quad [2]$$

with

X_{CO}	CO conversion	[−]
$g^*_{in/out,A}$	Corrected molar flow at the inlet or outlet of the anode	[mol s^{-1}]
$x^{\alpha}_{in/out,A}$	Molar fraction of component α at inlet or outlet	[−]

Likewise, the selectivity of O_2 toward CO_2 is calculated as the ration between the total amount of CO averaged converted and the total amount of moles converted, namely the sum of CO and H_2 that reacted

$$S_{CO_2,O_2} = \frac{g^*_{in,A} x^{CO}_{in} - g^*_{out,A} x^{CO}_{out}}{(g^*_{in,A} x^{CO}_{in} - g^*_{out,A} x^{CO}_{out}) + (g^*_{in,A} x^{H_2}_{in} - g^*_{out,A} x^{H_2}_{out})} \quad [3]$$

with

S_{CO_2,O_2} Selectivity of O_2 towards CO_2 [−]

The hydrogen recovery ratio relates the amount of hydrogen at the outlet of the reactor with the amount of hydrogen fed to the reactor and is calculated as,

$$\epsilon_{H_2} = \frac{g^*_{out,A} x^{H_2}_{out}}{g^*_{in,A} x^{H_2}_{in}} \quad [4]$$

with

ϵ_{H_2} Hydrogen recovery ratio [−]

Finally, the specific energy required for the CO conversion, which is a term suggested in Ref., 5 relates the amount of energy that is lost due to the undesired oxidation of hydrogen within the reactor with relation to the total amount of CO converted. This quantity is seen as a parameter that helps to compare the electrochemical reactor with the chemical reactor, from the technical point of view and is calculated as,

$$w_{CO} = \frac{(g^*_{in,A} x^{H_2}_{in} - g^*_{out,A} x^{H_2}_{out}) 2F U_{PEMFC} - U_{ECPrOx} I}{g^*_{in,A} x^{CO}_{in} - g^*_{out,A} x^{CO}_{out}} \quad [5]$$

with

w_{CO}	Specific energy required for the CO conversion	[J mol^{-1}]
U_{PEMFC}	Technical relevant voltage for PEM fuel cell operation	[V]
U_{ECPrOx}	Voltage of the ECPrOx reactor	[V]

In this contribution six different scenarios are presented and discussed in Results and discussion section. The operation parameter are given in Table I. For all of them the feed flow rate (357 ml/min) and relative humidity (70%) at the cathode side were kept constant. For both sides the back-pressure in the gas lines was set at 1.2 bar. The operating conditions for the cell and the anode side are presented below.

The operations conditions were selected in such a way, that only one parameter is modified in comparison with the reference case. Additionally, due to the configuration of the system, the lowest constant dew point achievable on the bubblers was 33 °C.

Results and Discussion

In the following section, the experimental results obtained for the six evaluated cases are presented. For this, the global descriptors, such as the polarization curve for galvanostatic and potentiostatic operation, as well as the frequency diagram for the autonomous oscillations are shown. Furthermore, since the curve depicts the global average results of several experiments, the progression of the anode overvoltage and the spatiotemporal behavior of the local current density for four selected galvanostatic experiments are also given. The local current density distribution is measured for two channels, however, since they are almost identical, only the result for one of the channels is displayed.

To complete the picture, the measured inlet and averaged outlet concentration are given. Since only the inlet and outlet concentration were measured, it was assumed that the average carbon monoxide concentration decreases linearly along the channel. Although this can't be proven in this study and may not be the case, it approximates the cell behavior.

The progression and spatiotemporal behavior under potentiostatic operation for all the cases is not presented here because after the steady state was reached, the total current density and the local current distribution did not change with time. However, a brief summary of the findings for potentiostatic operation is given in Spatiotemporal patterns during potentiostatic operation. At the end of the section, the results for the CO conversion and selectivity, as well as, the hydrogen recovery ratio and the specific energy required for CO oxidation are evaluated and discuss for all scenarios.

Reference case.—The reference case was selected in such a way that the only difference with the other five cases is a single operating condition. The purpose of it is to effectively compare and identify the features emerging due to a slight parameter modification.

In Fig. 2a the behavior of the anode overvoltage with increasing current density is given for potentiostatic and galvanostatic operation. The bifurcation current and voltage, is the point at which, during galvanostatic operation, the sustained and autonomous voltage oscillations arise. When the current density is lower than the bifurcation current, the anode overvoltage increases sharply and the behavior is identical for both control modes. Once the bifurcation current is reached, the slope of the curve decreases considerably for potentiostatic operation, (blue line).

For galvanostatic operation, once the bifurcation current is reached, autonomous oscillations in the cell voltage are observed. Therefore, the black line is split in two and the maximum and minimum values of the overvoltage under oscillatory behavior are collected. Additionally, the averaged temporal overvoltage is calculated and shown in Fig. 2a as a black dashed line. One of the most interesting features of the voltage oscillations is that contrary to most of the systems, the anode overvoltage losses due to the CO poisoning decrease with increasing current density for a portion of the curve and then increase again at a small slope as for potentiostatic operation. These features for the galvanostatic and potentiostatic operations have been partly observed and discussed by Refs. 16, 10, 5 for lumped and differential systems. However, in the experimental results of Kadyk et al.[10] and Nogueira et al.,[16] the last portion of the curve, where the overvoltage increases again, was not present; and for Pena et al.[5], it only emerged for CO inlet concentrations lower than 2000ppm, which is in accordance with the case presented here.

The oscillations frequency as a function of the current density are sketched in Fig. 2b. As has been previously shown by Ref., 5,10,13,16 after the bifurcation point, the frequency of the voltage oscillations decreases until a minimum value, and then increases again. Furthermore, Hanke-Rauschenbach et al.[9], explained that the period doubling, which occurs when the oscillations of the cell happen at two different main frequencies, is a consequence of the CO shock front; and arises when the oscillation period without the front is lower than the residence time within the reactor. Therefore, it is expected that the period doubling emerges with increasing current density and decreasing

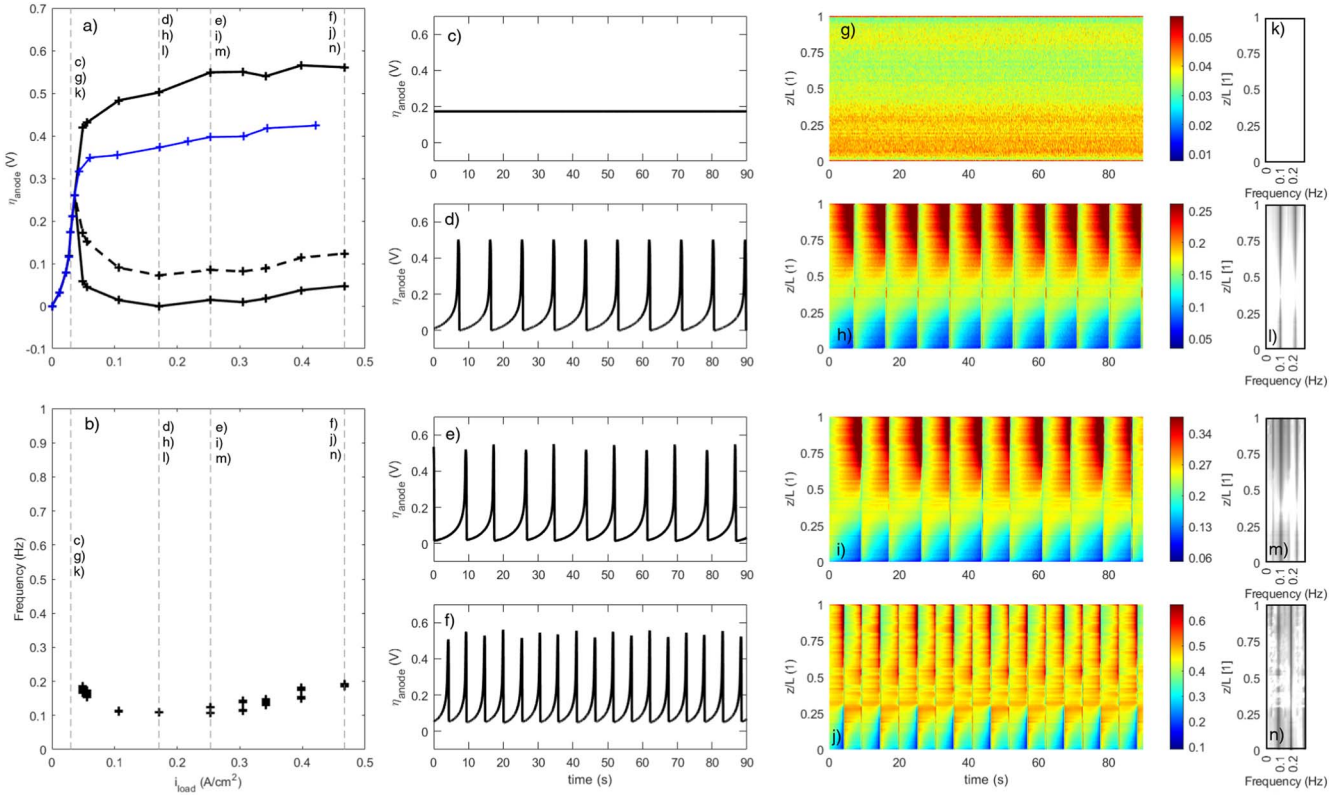

Figure 2. Experimental results for the reference case. (a) Polarization curve for galvanostatic (black) and potentiostatic (blue) operation. (b) Oscillation frequency of the oscillations for the evaluated current densities. (c)–(f) Overvoltage progression for the selected galvanostatic experiments. (g)–(j) Spatiotemporal patterns of the local current density for the selected experiments. (k)–(n) Temporal Fourier Spectrum of the local current densities.

Table I. Operating conditions for the series of experiments discussed in Results and Discussion section.

Scenario	T_{cell} [°C]	T_{dp} [°C]	F_{Anode} [ml/min]	CO_{in} [ppm]
Reference Case	40	33	357	932
Temperature Case	50	43	357	903
Low Flow Case	40	33	134	911
High Flow Case	40	33	892	911
Low CO Case	40	33	357	374
Low RH Case	50	33	357	938

feed flow rate. Period doubling and higher have been experimentally observed by Ref. 13, 16.

In Figs. 2c, 2g the progression of the anode overvoltage and the local current are given for a current slightly lower than the bifurcation current. Therefore, the overvoltage and the local current profile are not changing with time thus the Fourier Spectrum is empty an seen in 2k. Furthermore, in 2k for this case, the CO outlet concentration is 966 ppm, which is even higher than the inlet concentration. This happens because the critical overvoltage, at which water dissociates and CO oxidation can occur, has not been reached. As a consequence, only hydrogen is consumed and a CO concentration increase toward the outlet is occurring; thus, most of the current is obtained at the cell inlet where the CO concentration is the lowest.

When the current density increases, after the bifurcation point, sustained oscillations of the cell voltage are observed, due to the self-cleaning mechanism of the cell. At low anode overvoltage the catalyst sites at the anode are free and start being covered by the CO, thus the amount of free sites where hydrogen can react decreases; therefore the anode overvoltage increases until a critical overvoltage at which water dissociates, reacts with the adsorbed CO and the catalyst surface is freed. Since CO is continuously entering the cell, this self-cleaning process is continuously occurring, which makes the oscillations cyclic; a more detailed description of the process was given by Ref. 11.

These oscillations are well-defined and have a characteristic amplitude and frequency, see Fig. 2d. The local current density oscillates at the same frequency as the anode voltage. Contrary, to the profile observed in Fig. 2g, most of the current is produced at the second part of the cell where the CO concentration is lower, Figs. 2h, 2l. Furthermore, the current profile for every measurement increases toward the outlet of the cell, which indicates that the CO poisoning starts immediately at the inlet.

When the current is further increased, Figs. 2e, 2i, 2m, it can be observed that the oscillations have two main frequencies and two oscillations amplitudes, which has been previously characterized as period doubling by Ref. 9. In the local current distribution profile it can be identified by the frequency change among oscillations and the oscillating size of the high current section at the outlet of the cell. For the low frequency oscillation, the high current area (dark red) is bigger and the amplitude of the oscillation is lower. On the contrary, for the high frequency oscillations, the amplitude is higher and the

high current area is smaller. However, when comparing with the previous profile, where only one frequency is present, the spatio-temporal patterns are qualitatively similar.

As a final step for this case, the experimental results for the highest current density evaluated are collected in Figs. 2f, 2j, 2n. In the frequency graphic can be observed that the oscillation period is the same, however when looking at the progression of the global overvoltage it is noticeable that two different amplitudes are observed, as in the previous case that was characterized as period doubling. Furthermore, when the spatiotemporal patterns are considered, it is also noticeable that two different patterns that follow each other can be recognized.

This is the first time that such an oscillatory behavior is observed, where despite of the oscillations having the same frequency, two different amplitudes and patterns can be recognized. It cannot be classified as period doubling since the oscillations have the same frequency, however this behavior is also produced because the time required for the CO front is higher than the residence time in the reactor, which implies that the flow velocity is faster than the velocity at which the CO adsorbs on the catalyst. As a matter of fact, it is possible that the CO front is never able to cross the cell because it is consumed along the channel and therefore, the two different amplitudes have the same frequency, which is equivalent to the oscillation period without the front.

Temperature influence.—After evaluating the reference case, the temperature of the cell and bubblers were increased in such a way that the new operating temperature was 50 °C and the relative humidity was kept constant at 70%, equivalent to 43 °C as set temperature in the bubblers.

The experimental results are given in Fig. 3 and are depicted identical to the reference case. When comparing the polarization curves for galvanostatic operation, it is visible that for higher temperature, the bifurcation current and overvoltage are also higher, while the amplitude of the oscillations are at least 100 mV smaller for the same current density. For potentiostatic operation, the voltage loses are always smaller for the temperature case. On the contrary, for galvanostatic control, the averaged anode overvoltage is much lower for the reference case.

The influence of the temperature on the polarization curve has been previously evaluated by Zhang and Kadyk. In the work of Zhang et al.[6] the region at which the voltage oscillations appears was investigated, and they determined that with increasing temperature, increases as well the current density required for the appearance of the oscillations. This results was later confirmed by Kirsch et al.[13] In a later work,[1] they also observed that the CO outlet concentration increases with increasing temperature.

Likewise, Kadyk et al.[10] measured the polarization curve for a differential system with Pt anode fed with 100 ppm of CO at three different temperatures (40 °C, 60 °C and 80 °C) for galvanostatic and potentiostatic operation. For potentiostatic operation, they also observed that with increasing temperature, the voltage losses related with the CO poisoning decrease. This result, united with the fact that the CO outlet concentration is higher for higher temperature (Figs. 3g, 3h, 3i, 3j), implies that with increasing temperature the tolerance of the cell toward CO increases; thus, the adsorption of CO, together with the blockage of the surfaced area decreases. Therefore, for the purpose of hydrogen purification, the reactor should be operated at low temperatures.

For galvanostatic operation, in the results of Kadyk et al.[10], the amplitude of the oscillations decreases and the current density at the bifurcation point increases with increasing temperature. However, the anode overvoltage does not significantly depend on the temperature. In the results here presented, the difference between the overvoltage bifurcation is almost 50 mV.

The qualitative behavior of the frequency curve in Fig. 3b is similar to the one observed in the reference case. However, the frequency values are almost three times higher and the current

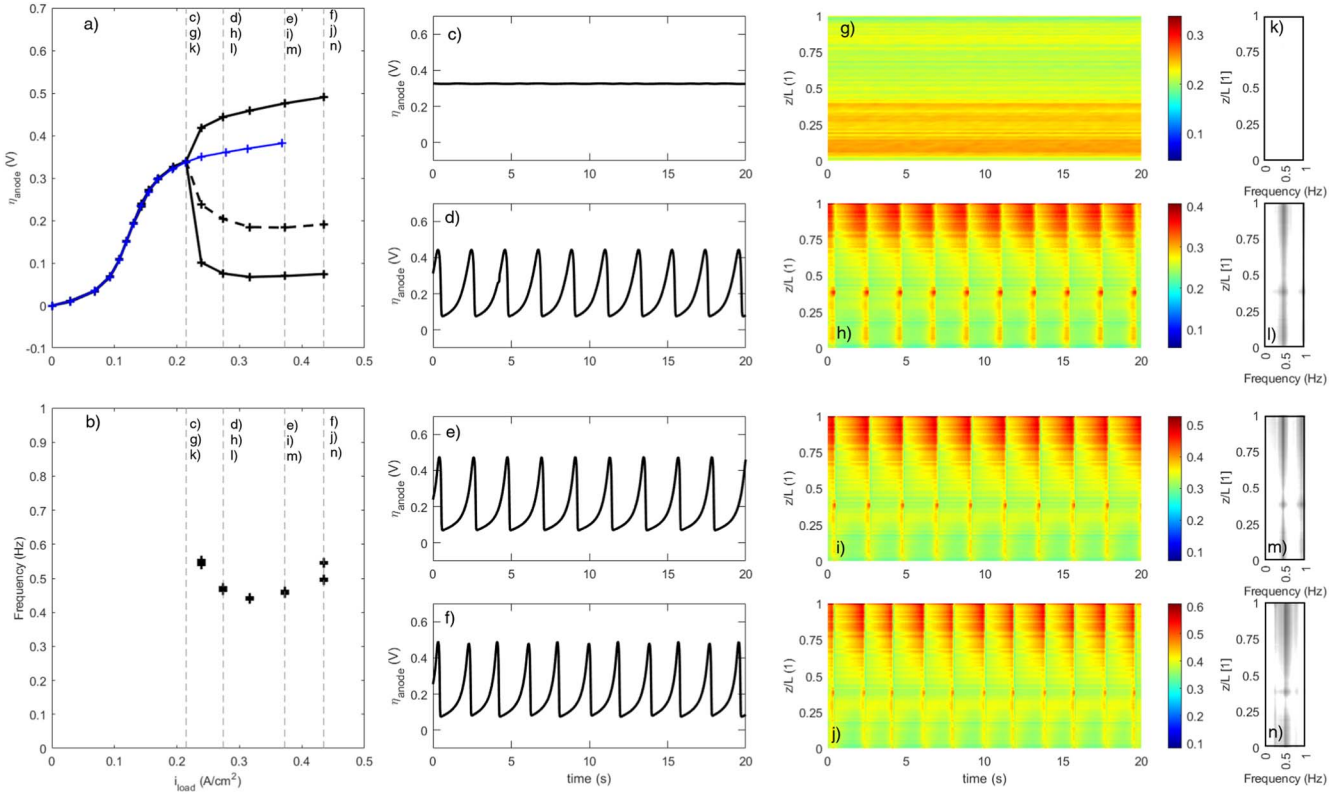

Figure 3. Experimental results for the temperature case. (a) Polarization curve for galvanostatic (black) and potentiostatic (blue) operation. (b) Oscillation frequency of the oscillations for the evaluated current densities. (c-f) Overvoltage progression for the selected galvanostatic experiments. (g-j) Spatiotemporal patterns of the local current density for the selected experiments. (k-n) Temporal Fourier Spectrum of the local current densities.

density at which the period doubling occurs is also higher; such a dramatic increase was also observed by Kirsch et al.[13] In the results of Kadyk et al.[10] the oscillation frequency also increases with temperature, but period doubling was not observed due to the configuration of the system. The period doubling is a consequence of the electrical coupling and the channel dynamics; since in the work of Kadyk a differential system was studied, the channel dynamics are insignificant and period doubling cannot arise.

As was observed in the reference case, after the bifurcation point, first one period oscillations appeared and then double period bifurcation arise. For the temperature case the sequence is the same, however the current at which the period is doubled is much higher as for the reference case. Since in both systems the feed flow rate is the same, the reason why at 50 °C the period doubling occurs so late is not related with the flow, but with the frequency of the oscillations. The system oscillates so fast that a CO front can be only formed when the flow rate has been reduced due to the consumption of the cell. Thus, increasing the time required for the front to cross the channel. Additionally, this period doubling is only evident when looking at the frequency plot, because the amplitude of the oscillations is the same.

When evaluating the spatiotemporal behavior of the cell, Figs. 3g, 3h, 3i, 3j, despite of the difference in the current density, the profile obtained for the experiment without voltage oscillations is the same for the temperature and the reference case. However, in this case the CO concentration at the outlet is lower than at the inlet. Thus, the critical voltage at which water dissociates has been reached but it does not have an impact on the local current distribution.

Once the oscillations emerge, the patterns obtained for the local current density profiles are very similar and the current gradient between the inlet and outlet of the cell is considerably smaller as for the reference case. Even for the last experiment, where period doubling is observed, the difference between the oscillations and patterns are insignificant, see Figs. 3f, 3j.

CO inlet concentration influence.—With respect to the reference case, for the low CO case just the CO inlet concentration was reduced. Similar experiments were carried out by Kadyk et al.[10] were they evaluated the polarization curve for a differential reactor under galvanostatic and potentiostatic control, with a CO inlet concentration varying between 20 and 200 ppm. They observed that for galvanostatic operation, with increasing CO inlet concentration, the bifurcation current decreases and the bifurcation overvoltage increases, for a Pt anode configuration. Additionally, in their results, for high current densities, the temporal averaged overvoltage was the same, independently on the CO inlet concentration. On the other hand, for potentiostatic operation, the anode overvoltage increased with the CO inlet concentration. These results are in agreement with our experimental findings, see Fig. 4a.

Likewise, Lu et al.[20] investigated the influence of the CO concentration in the feed (50-1000 ppm) on the oscillation period for an inhomogeneous system and noticed, that the frequency increases with increasing inlet concentration. Similarly, in the results here presented, Fig. 4b, the frequency is also lower. Furthermore, it can be also observed that the period doubling arises almost at the same current density. Such a period doubling was not studied by Lu et al. Ref. 24, however in their progression of the cell voltage, different amplitudes can be recognized for the same operating conditions, which indicates that as expected, channel dynamics were also present during their experiments.

When looking at the results of the selected experiments, Figs. 4c–4n, immediately before of the bifurcation point is reached, the local current is highest at the inlet, as was also the case in the previous figures. After the bifurcation point, the cell voltage and the local current oscillates at a single frequency, see Figs. 4d, 4h, 4l, and a clear stratification of the current toward the outlet is observed. In the next experiment, Figs. 4e, 4i, 4m, in the frequency diagram and in the cell voltage progression it can be observed that the anode overvoltage oscillates at a single frequency and amplitude; however, the local current distribution at the inlet of the cell oscillates at twice that frequency as observed in the Fourier spectrum, which means that two different patterns are observed. To the best knowledge of the authors, such a result has not been yet published.

Afterwards, with higher current densities, period doubling arises and different amplitudes and patterns can be identified. For the results presented in Figs. 4f, 4j, 4n, two different amplitudes and four different patterns can be observed in the progression of the anode overvoltage and spatiotemporal plot of the local current density, respectively. This is also confirmed by the the Fourier spectrum; the current profile is more heterogeneous and the high current area is also present in the middle of the cell, which indicates, as in the reference case, that most of CO has been consumed.

Feed flow rate influence.—To evaluate the influence of the feed flow rate, two additional cases were added to the reference case. The stoichiometric coefficients are 0.6, 1.6, and 4, for the low flow, reference and high flow case, respectively. From the experimental results in Figs. 5a and 6a, it can be observed that neither bifurcation point nor the amplitude of the oscillations are affected by the feed flow rate. Before the bifurcation point, the polarization curve is the same for the three cases. Afterwards, with increasing current densities, the difference among them increases, however a trend is not clear.

When looking at the frequency plots Figs. 5b and 6b, it can be observed that the frequency increases with the feed flow rate; which is explained by Lopes et al. by the fact that the CO adsorption is the main process controlling the oscillation frequency. Thus, if the total CO content decreases, decreases as well the frequency of the oscillations.

On the other hand, the frequency plots confirm the findings of Hanke-Rauschenbach,[9] which predicted that a more complex behavior is observed when the channel dynamics dominates the oscillatory behavior. Thus period doubling is observed at lower current densities when the feed flow rate is lower.[8,13] Additionally, the difference between the frequencies is much higher for lower feed flow rate, which was also observed by Kirsch et al.[13]

The overvoltage progression, the spatiotemporal behavior and temporal Fourier spectrum of the local current density for the low flow case are presented in Figs. 5c–5n. When the overvoltage is lower that the bifurcation overvoltage (Figs. 5c, 5g, 5k), the local current profile is identical to the ones observed for the other cases. No change in the global overvoltage or in the spatiotemporal pattern is observed.

After the bifurcation point (Figs. 5d, 5h, 5l), first homogeneous oscillations of the anode overvoltage are observed. A single frequency and amplitude are present. The local current density oscillates also at the single frequency and a clear stratification of the local current is observed; with increasing z, increases as well the local current density at all times.

With a further increase of the current density, the area where the period doubling emerges is reached (Figs. 5e, 5i, 5m). Here, the anode overvoltage oscillates at two different frequencies and two amplitudes are observed. The local current density also oscillates at two frequencies and two different patterns can be identified.

In the last experiment here presented for the low flow case (Figs. 5f, 5j, 5n) four frequencies and amplitudes can be identified from the progression of the anode overvoltage. Furthermore, in the local current density profile a characteristic pattern can be isolated for each of the frequencies. It is the first time that under steady state such a result is published.

For the high flow case, period doubling cannot be identified from the experimental results in Fig. 6b. This is expected because with an increase in the feed flow rate decrease the gradients along the channel. When the bifurcation current has not been reached, Figs. 6c, 6g, the local current profile behaves consistently as in the other cases evaluated previously.

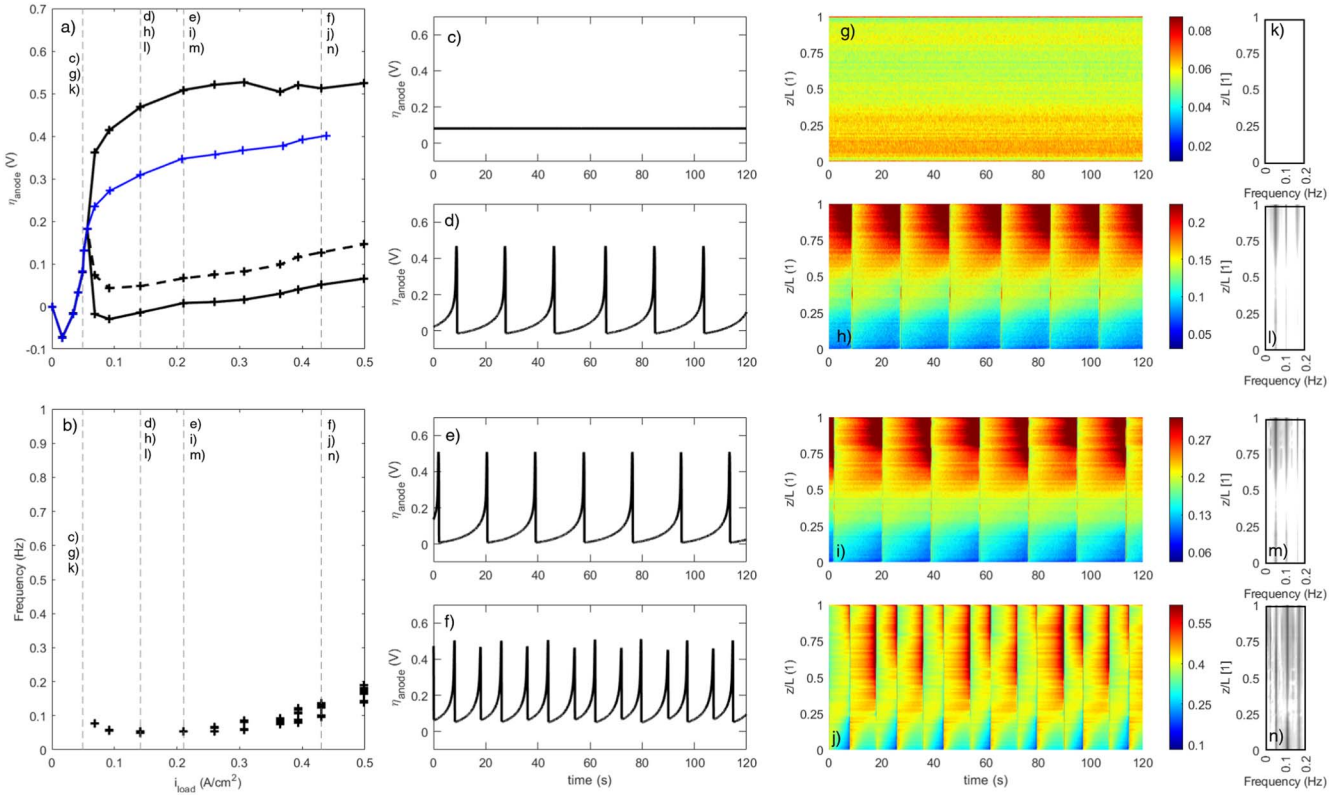

Figure 4. Experimental results for the low CO case. (a) Polarization curve for galvanostatic (black) and potentiostatic (blue) operation. (b) Oscillation frequency of the oscillations for the evaluated current densities. (c-f) Overvoltage progression for the selected galvanostatic experiments. (g-j) Spatiotemporal patterns of the local current density for the selected experiments. (k-n) Temporal Fourier Spectrum of the local current densities.

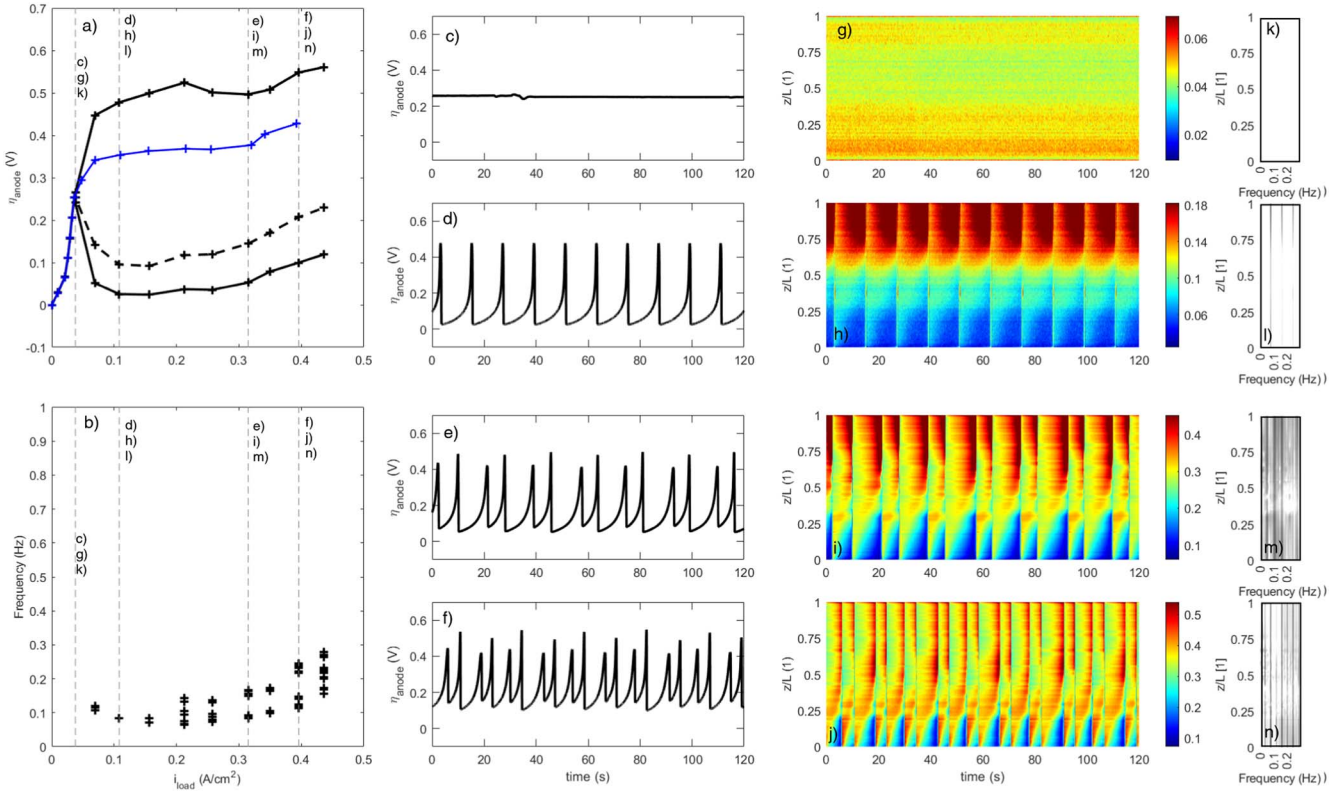

Figure 5. Experimental results for the low flow case. (a) Polarization curve for galvanostatic (black) and potentiostatic (blue) operation. (b) Oscillation frequency of the oscillations for the evaluated current densities. (c-f) Overvoltage progression for the selected galvanostatic experiments. (g-j) Spatiotemporal patterns of the local current density for the selected experiments. (k-n) Temporal Fourier Spectrum of the local current densities.

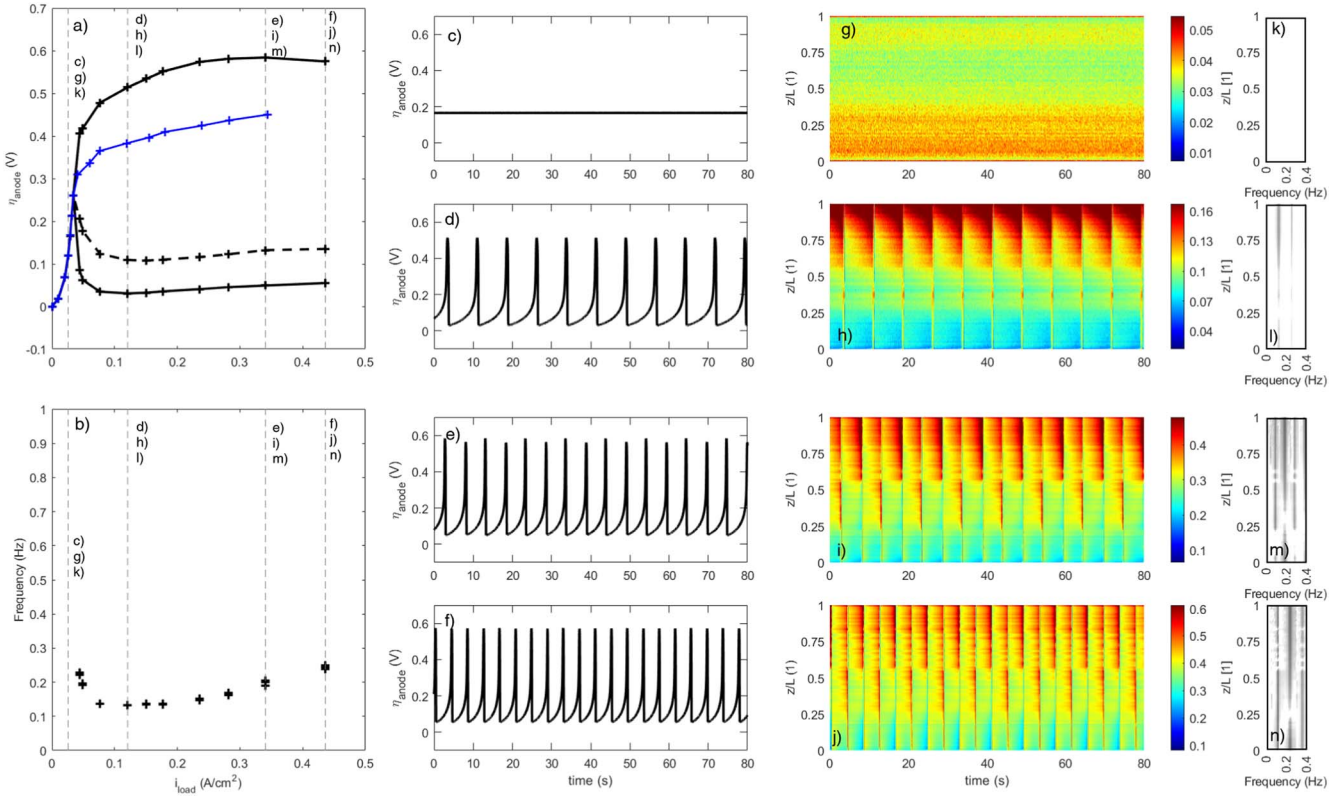

Figure 6. Experimental results for the high flow case. (a) Polarization curve for galvanostatic (black) and potentiostatic (blue) operation. (b) Oscillation frequency of the oscillations for the evaluated current densities. (c-f) Overvoltage progression for the selected galvanostatic experiments. (g-j) Spatiotemporal patterns of the local current density for the selected experiments. (k-n) Temporal Fourier Spectrum of the local current densities.

Furthermore, when the current is increased, Figs. 6d, 6h, the anode overvoltage oscillates at a single frequency and amplitude; which also occurs in the other cases. Moreover, there is a clear stratification in the local current profile and a single pattern with the same frequency as the anode overvoltage can be observed. Despite the stratification, the absolute difference in the current density between the inlet and outlet of the cell is not as high as for the low flow case. This is related with the fact that the CO content along the channel does not differ as much as for the previous case.

However when looking at the progression of the anode overvoltage and the spatiotemporal behavior of the local current density for the third experiment in Figs. 6e, 6i, it is obvious that two amplitudes and patterns can be recognized. Additionally, for the fourth experimental result in Figs. 6f, 6j, a single amplitude can be observed but two different patterns are formed in the spatiotemporal plot, which is consistent with the appearance of new frequencies in the Fourier spectrum.

Finally, with increasing flow rate, increases as well the anode outlet CO concentration, as have been already shown by Ref. 1, 21, 24. This occurs because the total amount of CO fed to the reactor increases linearly with the feed flow rate, if the concentration is kept constant. Thus, if the area of the reactor is not scaled up, it is to expect that the conversion within the reactor decreases proportionally.

Relative humidity influence.—In comparison with the reference case, for the relative humidity case, the cell temperature was increased to 50 °C, while the temperature of the bubblers was kept at 33 °C. By increasing the cell temperature, the partial pressure, as well as the concentration of the water decreases, despite the fact that its total amount is kept constant.

As can be observed in Figs. 7a, 7b, the oscillation frequency as well as the bifurcation current and overvoltage increase in comparison with the reference case. However, the anode overvoltage before the bifurcation point is lower than the one reported for the reference case under potentiostatic operation. After the bifurcation point, the temporal averaged overvoltage is higher for galvanostatic and potentiostatic operation when the relative humidity is lower.

On the other hand, when comparing with the temperature case, it can be observed that the bifurcation overvoltage remains constant, the frequency of the oscillations are in the same range and the bifurcation current decreases when the relative humidity decreases. Additionally, for the low relative humidity case the period doubling is not observed and for all the experiments the anode overvoltage oscillates at a single amplitude and frequency, see Figs. 7b–7f. This is also confirmed by very clear Fourier spectrum for all experiments along the channel.

In previous studies, Zhang et al.[1] evaluated the influence of the humidification on an ECPrOx reactor at ambient temperature and noticed that the difference in the performance of the reactor was not significantly impacted. This observation is contradictory with the results here presented, and can be explained by the fact, that in their experiments the cathode feedstock contained oxygen. Thus water was produced within the reactor as by product, which increased the water partial pressure on the catalyst surface and the channel.

Analogously, in 2013 Kirsch et al.[13] investigated the influence of the humidification in an ECPrOx reactor with the same cathode configuration as in the present work. They found out that with decreasing relative humidity, the limiting current of the cell also decreases. They observed the same results for cells that did not contain CO in the anode feed and they related the significantly loss in cell performance with anode dry out. For the experiments presented here, the maximum current that can be produced by the reactor was 0.25 A/cm^2, almost half of the standard case.

Furthermore, as has been stated previously, the critical voltage represents the voltage at which water dissociates. Water dissociation is required to oxidize the CO that is adsorbed on the surface. If the water concentration decreases, as in this case, CO cannot be as easily

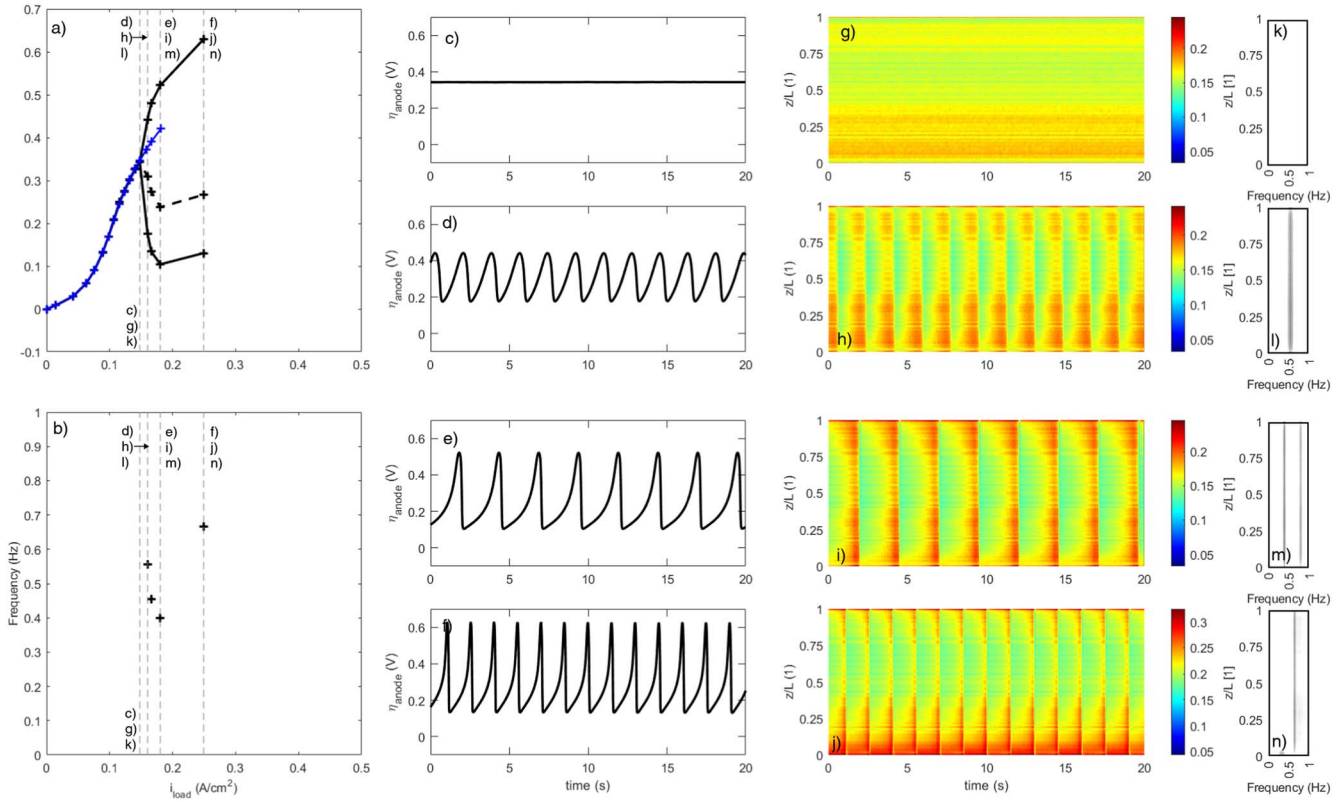

Figure 7. Experimental results for the low relative humidity case. (a) Polarization curve for galvanostatic (black) and potentiostatic (blue) operation. (b) Oscillation frequency of the oscillations for the evaluated current densities. (c-f) Overvoltage progression for the selected galvanostatic experiments. (g-j) Spatiotemporal patterns of the local current density for the selected experiments. (k-n) Temporal Fourier Spectrum of the local current densities.

oxidized as for the other cases, which means that the surface will remain blocked by the adsorbed CO. This, in conjunction with the gradient of CO concentration toward the outlet, explains why in the spatiotemporal graphics of the local current density presented in Figs. 7h–7j, most of the current is produced at the inlet and outlet of the cell once the oscillations emerged. Additionally, it is observed that the CO outlet concentration is not considerably affected by the increase in current density (Figs. 7k–7n) and that the amount of CO that reacted is much lower as for the other cases.

Moreover, when comparing with the previous cases, the local current profiles are considerably homogeneous which suggests that the coupling among the sites is stronger; thus current stratification is not observed. These findings contradict the modeling results presented by Hanke-Rauschenbach et al.[9], where they showed that by increasing the membrane resistance an uncoupling effect among the reaction sites can be observed, which would produce a chaotic behavior on the local current profile. However, in their simulations they modify the membrane resistance without altering the thickness of the membrane or the water concentration. Thus, their results cannot be extrapolated nor compared with the ones presented here.

Spatiotemporal patterns during potentiostatic operation.—Until now, only the results for galvanostatic operation have been presented. As has been stated before, the results for potentiostatic operation are not as exciting as the previously shown because under steady state the anode overvoltage and the local current profile are constant with time. However, for the sake of completeness the results obtained for the reference case are presented in Fig. 8.

As has been seen in the cases presented before, when the bifurcation point has not been reached, the current is mostly produced at the inlet of the cell and the CO concentration increases toward the outlet of the cell because only hydrogen is reacting.

After the bifurcation point, it can be observed how the current profiles are changing and shifting toward the outlet of the cell. The current stratification emerges with increasing current density. The changes between each step are very noticeable even when the increase in the anode overvoltage is small.

The same profiles were obtained for all the cases with increasing anode overvoltage with exception of the relative humidity case. For the latter, only the profile observed in Fig. 8g was present even for the highest voltage experiment. Thus, the loss of humidity produces that for the low relative humidity case the local current profiles are not altered with increasing current density and anode overvoltage.

This is the first time that the spatiotemporal behavior of the local current density under steady state is presented for potentiostatic operation. In a previous work, Kirsch et al.[13] reported the presence of pulses and turbulence for an analogous system; however they performed voltage scans and load jumps. Based on these results, it is very likely that the phenomena reported by them, was the response of the cell to the load dynamics. During this study, the load dynamics were not evaluated nor considered.

Reactor performance.—The reactor performance for all scenarios is here evaluated. For this, the conversion, selectivity, hydrogen recovery and specific energy required for CO oxidation are calculated and compared under galvanostatic and potentiostatic control, as a function of the current density.

In Fig. 9 the results obtained for the reference case are presented. As was discussed at the begining of the section, once the critical potential for water dissociation is reached, the averaged CO outlet concentration decreases with increasing current density for galvanostatic and potentiostatic control. However, due to the potential oscillations, the CO conversion and selectivity is higher for the galvanostatic case.

Regarding the hydrogen recovery ratio, it can be observed that, since the amount of CO present in the feedstock is just traces, on one side the difference between galvanostatic and potentiostatic control is negligible and on the other, that most of the current produced in the cell is coming from the hydrogen oxidation.

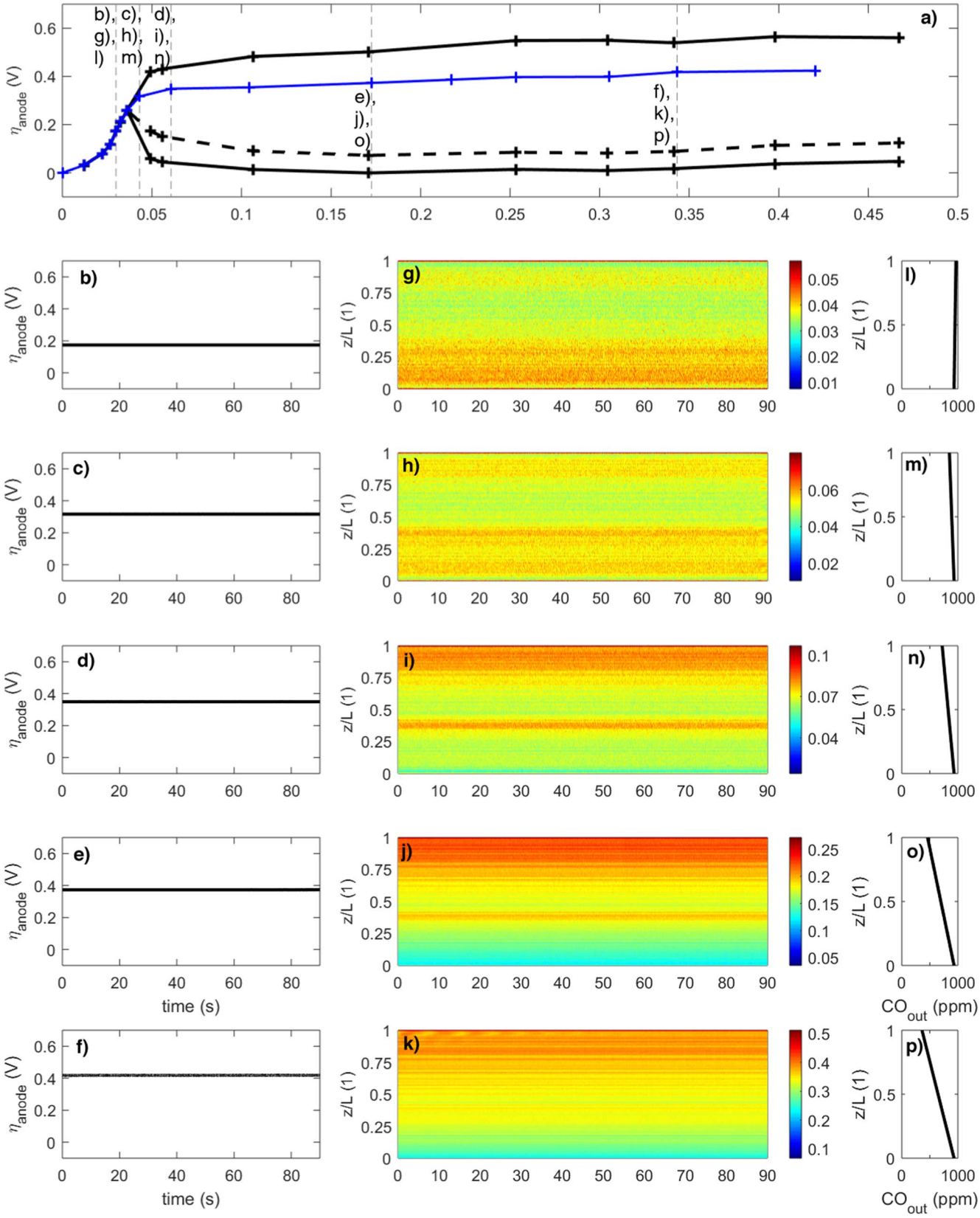

Figure 8. Experimental results for the reference case. (a) Polarization curve for galvanostatic (black) and potentiostatic (blue) operation. (b-f) Overvoltage progression for the selected potentiostatic experiments. (g-k) Spatiotemporal patterns of the local current density for the selected experiments. (l-p) Measured inlet and outlet concentration during the experiments. The two points are connected with a straight line.

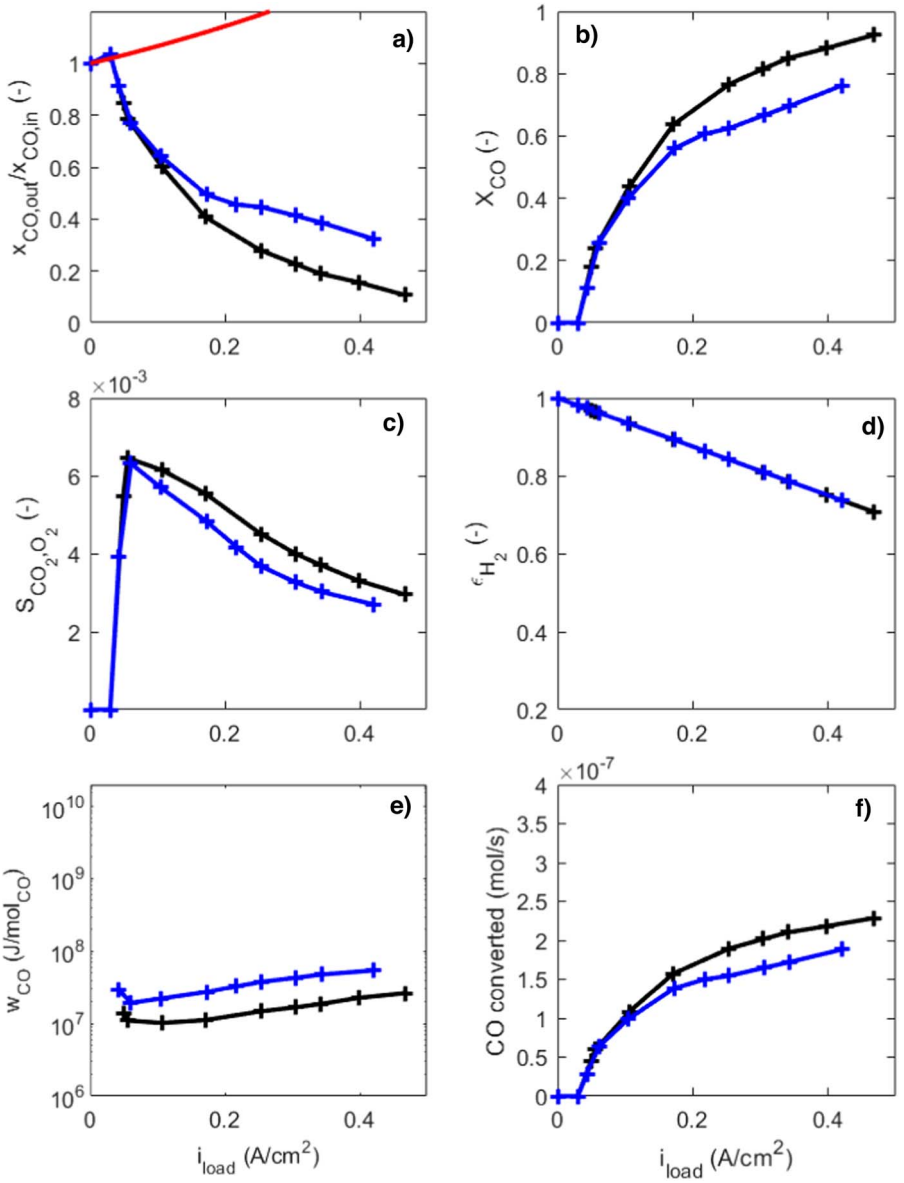

Figure 9. Reactor performance for the reference case under galvanostatic (black) and potentiostatic (blue) operation as a funcion of the current density. (a) Ratio between outlet and inlet concentration of CO. (b) CO conversion. (c) selectivity of O_2 toward CO_2. (d) Hydrogen recovery ratio. (e) Specific energy required for CO conversion. (f) Moles of CO converted.

Additionally, when observing the behavior of the specific energy required for the CO oxidation, it is clear that under galvanostatic control the energy required is much lower; mainly due to the fact that, due to the oscillations, the temporal averaged anode overvoltage is much lower than when compared with potentiostatic control.

This results are in agreement with the experiments carried out by Ref. 5 where a well-mixed ECPrOx reactor was evaluated. The qualitative behavior of the reactors are the same, however, the PFTR presented here outperforms the well mixed reactor in CO conversion as modeled by Ref. 3 and experimentally evaluated by Ref. 2. Furthermore, a special effect related with the presence of two or more frequencies or amplitudes is not observed in the global performance of the reactor.

In the following, the technical diagrams for the different cases are presented. For this, the selectivity, hydrogen recovery ratio and specific energy required for the CO conversion are plotted as a function of the moles of CO converted. The latter is used as *x*-axis because the amount of CO fed to the reactor is not constant for all experiments, and this allows a fair comparison among the scenarios. A similar analysis was presented by Ref. 5 using the CO conversion as *x*-Axis, since the total flow was constant for all experiments.

The technical diagrams for the reference case are presented in Fig. 10. A red line is include in all of them and represents the total amount of CO fed to the reactor, which means that the closer the evaluated points are to the red line, higher is the conversion. Moreover, for the three figures, the behavior between potentiostatic and galvanostatic control diverges after the bifurcation point, being the performance under galvanostatic control better. Furthermore, a maximum and a minimum can be observed for the selectivity and specific energy require curves, respectively.

When comparing with the technical diagrams obtained for the temperature case presented in Fig. 11, it is clear that the performance of the reactor is better at lower temperatures because the conversion, selectivity and hydrogen recovery ratio are higher. Similarly, the energy required for CO oxidation is lower which can be explained by the higher selectivity and lower averaged anode overvoltage.

Furthermore, the values obtained for the temperature case are in agreement with the findings presented in Ref., 5 where the energy

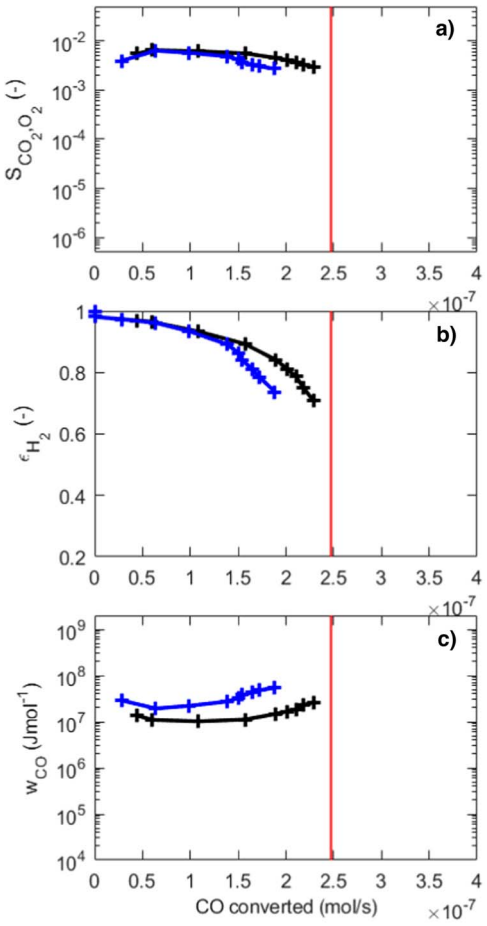

Figure 10. Technical diagrams for the reference case under galvanostatic (black) and potentiostatic (blue) operation as a function of the moles of CO converted. (a) Selectivity of O_2 toward CO_2. (b) Hydrogen recovery ratio. (c) Specific energy required for CO conversion.

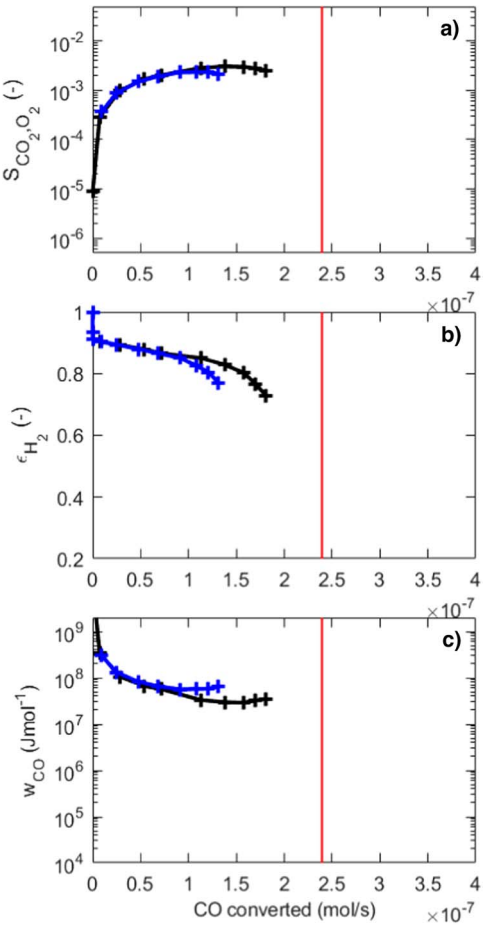

Figure 11. Technical diagrams for the temperature case under galvanostatic (black) and potentiostatic (blue) operation as a function of the moles of CO converted. (a) Selectivity of O_2 toward CO_2. (b) Hydrogen recovery ratio. (c) Specific energy required for CO conversion.

required for the CO oxidation for the well mixed reactor is in the same order of magnitude as what was found in this study for the spatially distributed reactor.

Looking at the results obtained for the low CO case, presented in Fig. 12, it can be observed that, in comparison to the reference case, the amount of CO converted is considerably lower because the amount of the CO fed to the reactor is also lower. Furthermore, the selectivity is lower and the energy required for the CO conversion is higher. On the contrary, even with lower selectivity for the low CO case, the conversion is higher, reaching almost full conversion for the galvanostatic case at $0.5\frac{A}{cm^2}$. These findings confirm the observations presented by Ref., 5 where the performance of a well-mixed reactor is evaluated for several CO concentration values.

For the low flow case in Fig. 13, the total amount of CO fed to the reactor is almost the same as for the low CO case but the performance of the reactor is better regarding CO conversion, selectivity and energy required for the CO oxidation; due to the higher concentration of CO. On the contrary, when looking at the hydrogen recovery ratio, the ratio is lower because the amount of hydrogen fed is one third while the current density is the same.

On the other hand, when comparing the high flow results presented in Fig. 14 with the reference and low flow case, it can be observed that the selectivity and the hydrogen recovery ratio increases with increasing flow rate while the energy required decreases. However, when looking at the conversion, this is higher when the flow decreases because the amount of CO to be converted is lower. For the high flow case, the red line is no visible in Fig. 14 since it lays further in the *x*-axis.

Finally, when evaluating the results for the low relative humidity case, see Fig. 15, it is evident that the curves are the same but shorter as for the temperature case. These indicate that the lack of water has a higher impact on the anode overpotential, the local current density profile and conversion, than what it has on the selectivity, hydrogen recovery ratio and energy required for the CO oxidation.

Conclusions and Outlook

In the present contribution, the influence of the operating parameters on the CO outlet concentration, the reactor performance and the local current profile under potentiostatic and galvanostatic operation were evaluated for a spatially distributed ECPrOx reactor.

For all the scenarios evaluated, it was observed that until the bifurcation point, the behavior of the cell is the same independently of the control type imposed by the load. Afterwards, the anode overvoltage under potentiostatic operation is always higher than the temporal averaged anode overvoltage under galvanostatic control. Additionally it was seen that for both type of control, the CO outlet concentration decreases always with increasing current density; however when comparing the control, the CO outlet concentration is always higher for potentiostatic operation. Similarly, under galvanostatic operation the reactor performance, namely conversion, selectivity, and specific energy required for CO oxidation, is always better than for potentiostatic control under the same operation conditions.

For galvanostatic operation, right after the bifurcation point, the oscillations of the anode overvoltage are characterized by a single frequency and amplitude. The local current oscillates at the same

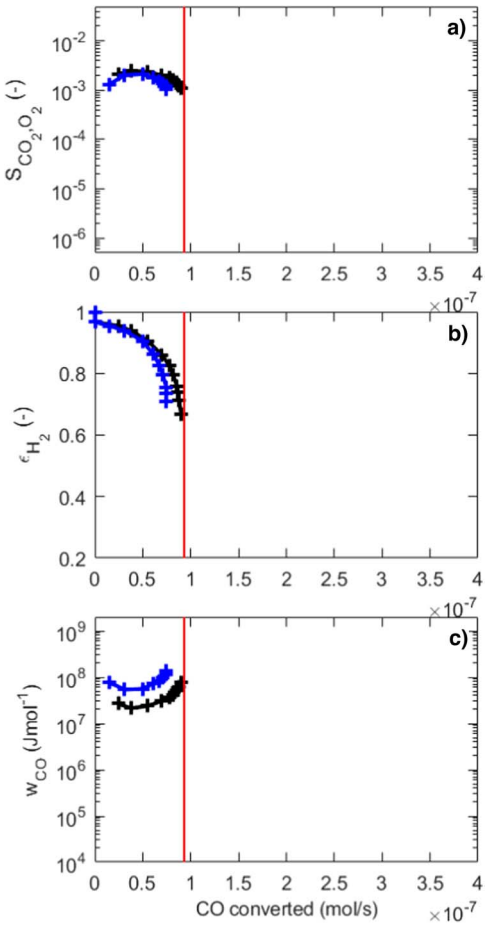

Figure 12. Technical diagrams for the low CO case under galvanostatic (black) and potentiostatic (blue) operation as a function of the moles of CO converted. (a) Selectivity of O_2 toward CO_2. (b) Hydrogen recovery ratio. (c) Specific energy required for CO conversion.

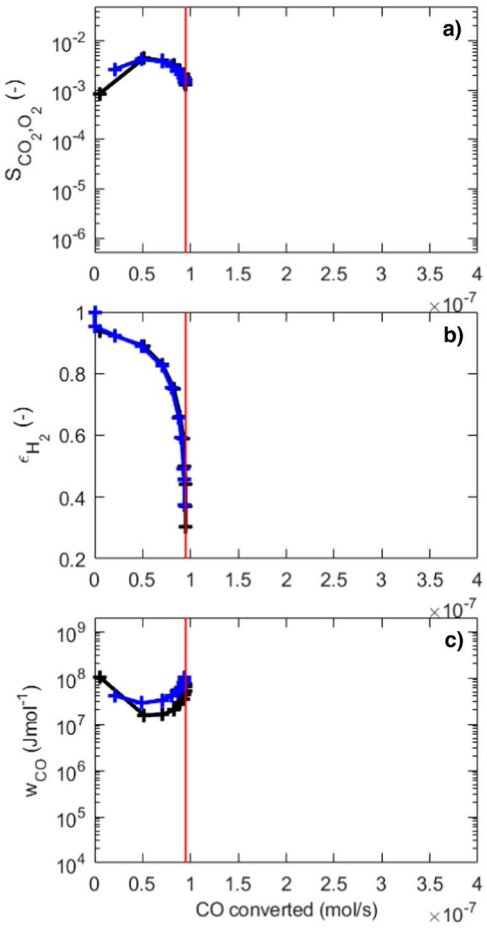

Figure 13. Technical diagrams for the low flow case under galvanostatic (black) and potentiostatic (blue) operation as a function of the moles of CO converted. (a) Selectivity of O_2 toward CO_2. (b) Hydrogen recovery ratio. (c) Specific energy required for CO conversion.

frequency and a single pattern is formed during this period. With increasing current density, the frequency of the oscillations decreases up to a minimum value and increases again.

After this minimum, the oscillations of the anode overvoltage can be characterized by more than one frequency and one or more amplitudes, a phenomena which is called period doubling. Additionally, it was also observed that a variety of cases could also arise during the oscillations. For instance, oscillations of the anode overvoltage with a single frequency and two amplitudes, whose local current distribution oscillates at half the frequency; or an anode overvoltage oscillating at a single frequency and amplitude, while the local current oscillates at one half of the frequency. This high diversity of profiles on the local current density appears to not have an effect on the CO-oxidation performance of the electrochemical reactor, since the curves behave monotonically and analogously to the potentiostatic case.

For the potentiostatic operation it was found that under steady state, the global and local current do not change with time; however, a characteristic sequence in the spatiotemporal behavior was observed for all the cases. Initially, when the critical voltage has not been reached, most of the current is produced at the inlet of the cell. After the bifurcation point, the local current hotspot shifts toward the outlet of the cell until a clear stratification of the local current profile can be observed. This transition was present for all the cases with exception of the low relative humidity scenario.

With increasing temperature, increases as well the bifurcation current, the bifurcation voltage and the oscillations frequency. For potentiostatic operation, the anode overvoltage is lower at higher temperatures thanks to the increase in the hydrogen oxidation rate and the shift in the adsorption equilibrium. For galvanostatic operation, the temporal averaged overvoltage is lower when the temperature decreases; on the contrary, the amplitude of the oscillations as well as the amount of CO consumed increase. Additionally, it was observed that with increasing temperature, the patterns formed by the oscillations of the local current density become more homogeneous and period doubling arises at higher current densities.At the same time, the reactor performance decreases, express as a reduction in the conversion and the selectivity, while the specific energy required for CO oxidation increases.

A decrease in the CO inlet concentration decreases as well the bifurcation voltage and the frequency of the oscillations. On the contrary, the bifurcation current increases, as well as, the anode overvoltage under potentiostatic control. However for galvanostatic control, the CO inlet concentration does not have an impact on the anode overvoltage nor on the occurrence of period doubling. Likewise, the spatiotemporal behavior of the local current is also not considerably affected. On the other hand, when looking at the reactor performance, a reduction in the CO concentration increases the conversion while reducing the selectivity and the total amount of CO converted. This results corroborate the finding of Ref. 5.

The feed flow rate has a very slight influence on the polarization curve for both control modes. However, it does have an impact on the frequency of the oscillations and the local current density profile. When the feed flow rate is low, the frequency is lower and the period doubling arises at a lower current density. Additionally, a variety of frequencies and amplitudes are present and the difference between the local current at the inlet and outlet is the highest. When the flow is high the difference

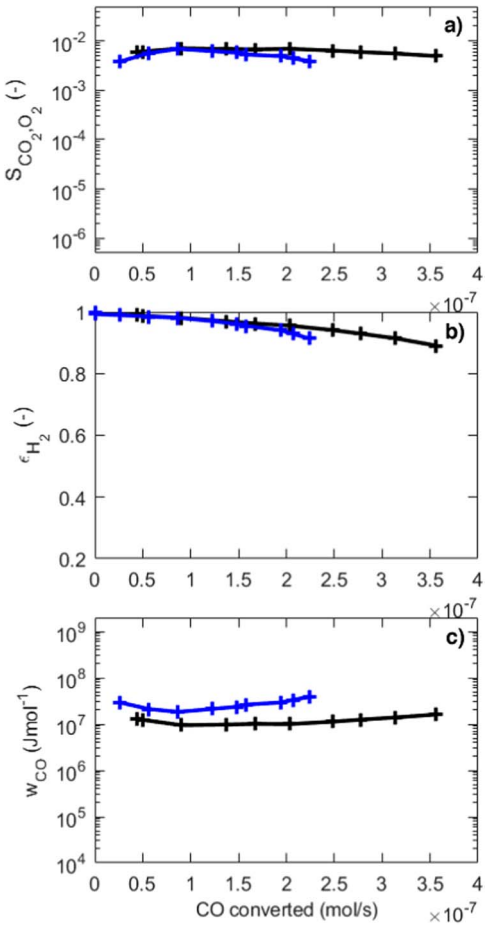

Figure 14. Technical diagrams for the high flow case under galvanostatic (black) and potentiostatic (blue) operation as a function of the moles of CO converted. (a) Selectivity of O_2 toward CO_2. (b) Hydrogen recovery ratio. (c) Specific energy required for CO conversion.

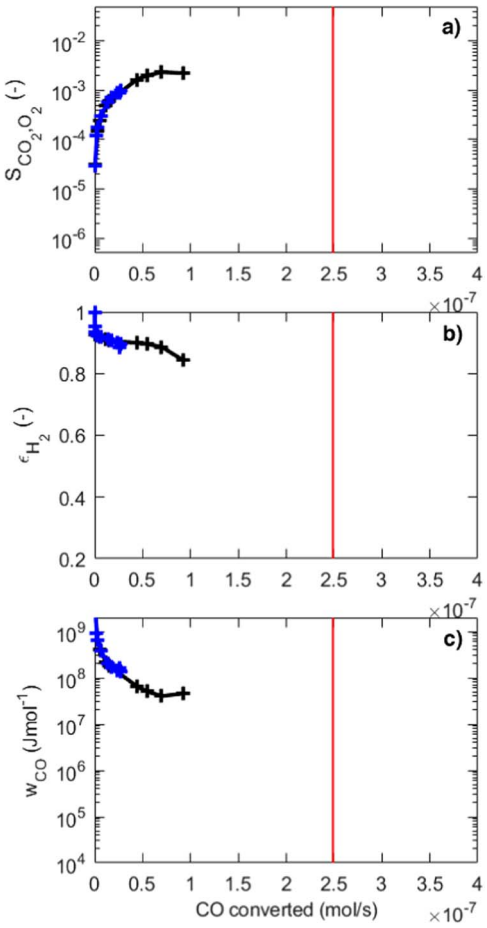

Figure 15. Technical diagrams for the low relative humidity case under galvanostatic (black) and potentiostatic (blue) operation as a function of the moles of CO converted. (a) Selectivity of O_2 toward CO_2. (b) Hydrogen recovery ratio. (c) Specific energy required for CO conversion.

of the frequencies and amplitudes are much smaller, but the period doubling phenomena does not disappear. The CO outlet concentration is for this scenario higher; however, with increasing flow increases as well the CO converted, the selectivity and the hydrogen recovery ratio, while decreasing the specific energy required for the CO oxidation.

When the relative humidity is low, a decrease in the cell performance,expressed as a lower current limit and a higher anode overvoltages, is observed. However, when comparing the reactor performance curves, the selectivity, the hydrogen recovery ratio and the energy required is the same as for the reactor with higher humidification. Additionally, contrary to the other scenarios, the current is produced mostly at the inlet of the cell and the variation of the local current with time is very low.

The systematic evaluation here presented is a first step into the evaluation of the technical feasibility of an ECPrOx reactor. For this, is still necessary to consider the impact of the sustained oscillations of the anode overvoltage on the long term behavior of the reactor should be further studied.

Acknowledgments

The authors gratefully acknowledge the financial support from the Deutsche Forschungsgemeinschaft (DFG), grant No. HA 6841/1-1.

ORCID

Ivonne Karina Peña Arias https://orcid.org/0000-0001-7220-0245
Richard Hanke-Rauschenbach https://orcid.org/0000-0002-1958-307X
Kai Sundmacher https://orcid.org/0000-0003-3251-0593

References

1. J. Zhang and R. Datta, "Electrochemical preferential oxidation of CO in reformate." *J. Electrochem. Soc.*, **152**, A1180 (2005).
2. H. Lu, L. Rihko-Struckmann, R. Hanke-Rauschenbach, and K. Sundmacher, "Improved electrochemical CO removal via potential oscillations in serially connected PEM fuel cells with PtRu anodes." *Electrochim. Acta*, **54**, 1184 (2009).
3. R. Hanke-Rauschenbach, C. Weinzierl, M. Krasnyk, L. Rihko-Struckmann, H. Lu, and K. Sundmacher, "Operating behavior and scale-up of an ECPrOx unit for CO removal from reformate for PEM fuel cell application." *J. Electrochem. Soc.*, **156**, B1267 (2009).
4. P. Heidebrecht, R. Hanke-Rauschenbach, A. Joerke, and K. Sundmacher, "On the design of cascades of ECPrOx reactors for deep CO removal from reformate gas." *Chem. Eng. Sci.*, **67**, 43 (2012).
5. I. K. Pena Arias, K. Sundmacher, and R. Hanke-Rauschenbach, "Influence of the autonomous oscillations and the co concentration on the performance of an ecprox reactor." *Electrochim. Acta*, **251**, 612 (2017).
6. J. Zhang and R. Datta, "Sustained potential oscillations in proton exchange membrane fuel cells with PtRu as anode catalyst." *J. Electrochem. Soc.*, **149**, A1423 (2002).
7. J. Zhang and R. Datta, "Higher power output in a PEMFC operating under autonomous oscillatory conditions in the presence of CO." *Electrochem. Solid-State Lett.*, **7**, A37 (2004).
8. A. Mota, P. P. Lopes, E. A. Ticianelli, E. R. Gonzalez, and H. Varela, "Complex oscillatory response of a PEM fuel cell fed with H2/CO and oxygen." *J. Electrochem. Soc.*, **157**, B1301 (2010).
9. R. Hanke-Rauschenbach, S. Kirsch, R. Kelling, C. Weinzierl, and K. Sundmacher, "Oscillations and pattern formation in a PEM fuel cell with Pt/Ru anode exposed to H2/CO mixtures." *J. Electrochem. Soc.*, **157**, B1521 (2010).
10. T. Kadyk, S. Kirsch, R. Hanke-Rauschenbach, and K. Sundmacher, "Autonomous potential oscillations at the Pt anode of a polymer electrolyte membrane fuel cell under CO poisoning." *Electrochim. Acta*, **56**, 10593 (2010), Selected Papers from the LXI ISE Meeting, Nice, France, 2010.

11. S. Kirsch, R. Hanke-Rauschenbach, A. El-Sibai, D. Flockerzi, K. Krischer, and K. Sundmacher, "The S-shaped negative differential resistance during the electro-oxidation of H2/CO in polymer electrolyte membrane fuel cells: modeling and experimental proof." *The Journal of Physical Chemistry C*, **115**, 25315 (2011).
12. S. Kirsch, R. Hanke-Rauschenbach, and K. Sundmacher, "Analysis of spatio-temporal pattern formation in a PEM fuel cell with Pt/Ru anode exposed to H2/CO mixtures." *J. Electrochem. Soc.*, **158**, B44 (2011).
13. S. Kirsch, R. Hanke-Rauschenbach, B. Stein, R. Kraume, and K. Sundmacher, "The electro-oxidation of H2,CO in a model PEM fuel cell: oscillations, chaos, pulses." *J. Electrochem. Soc.*, **160**, F436 (2013).
14. C. G. Farrell, C. L. Gardner, and M. Ternan, "Experimental and modelling studies of CO poisoning in PEM fuel cells." *J. Power Sources*, **171**, 293 (2007).
15. Y. Matsuda, T. Shimizu, and S. Mitsushima, "Adsorption behavior of low concentration carbon monoxide on polymer electrolyte fuel cell anodes for automotive applications." *J. Power Sources*, **318**, 8 (2016).
16. J. A. Nogueira and H. Varela, "Voltage oscillations in a polymer electrolyte membrane fuel cell with pd-pt/c and pd/c anodes." *ChemistryOpen*, **6**, 629 (2017).
17. V. F. Valdes-Lopez, T. Mason, P. R. Shearing, and D. J. L. Brett, "Carbon monoxide poisoning and mitigation strategies for polymer electrolyte membrane fuel cells—a review." *Prog. Energy Combust. Sci.*, **79**, 100842 (2020).
18. R. Hanke-Rauschenbach, M. Mangold, and K. Sundmacher, "Nonlinear dynamics of fuel cells: a review." *Rev. Chem. Eng.*, **27**, 23 (2011).
19. B. Shabani, M. Hafttananian, S. Khamani, A. Ramiar, and A. A. Ranjbar, "Poisoning of proton exchange membrane fuel cells by contaminants and impurities: Review of mechanisms, effects, and mitigation strategies." *J. Power Sources*, **427**, 48 (2019).
20. H. Lu, L. Rihko-Struckmann, and K. Sundmacher, "Spontaneous oscillations of cell voltage, power density, and anode exit co concentration in a pem fuel cell." *Phys. Chem. Chem. Phys.*, **13**, 18179 (2011).
21. P. P. Lopes, B. C. Batista, G. A. Saglietti, H. Varela, and E. A. Ticianelli, "Real-time determination of co2 production and estimation of adsorbate coverage on a proton exchange membrane fuel cell under oscillatory operation." *J. Solid State Electrochem.*, **17**, 1851 (2013).
22. R. Hanke-Rauschenbach, S. Kirsch, and K. Sundmacher, "Spatiotemporal pattern formation in an electrochemical membrane reactor during deep co removal from reformate gas." *XXI European Symposium on Computer Aided Process Engineering of Computer Aided Chemical Engineering, vol 29*, ed. E. N. Pistikopoulos, M. C. Georgiadis, and A. C. Kokossis et al. (Amsterdam) (Elsevier)p. 201 (2011).
23. I. K. Pena Arias, P. Trinke, R. Hanke-Rauschenbach, and K. Sundmacher, "Understanding PEM fuel cell dynamics: The reversal curve." *Int. J. Hydrogen Energy*, **42**, 15818 (2017).
24. H. Lu, L. Rihko-Struckmann, R. Hanke-Rauschenbach, and K. Sundmacher, "Dynamic Behavior of a PEM Fuel Cell During Electrochemical CO Oxidation on a PtRu Anode." *Top. Catal.*, **51**, 89 (2008).